X-ray Magnetic Circular Dichroism and Near-Edge X-ray Absorption Fine Structure of Buried Interfacial Magnetism Measured by using a Scanning Tunneling Microscope Tip

H. Chang[1,2], N. Shirato[3], Y. Zhang[3], J. Hoffman[4], D. Rosenmann[3], J.W. Freeland[1], A. Bhattacharya[3,5], V. Rose[1,3], S.-W. Hla[2,3,]*

[1]*Advanced Photon Source, Argonne National Laboratory, 9700 S. Cass Ave., Argonne, IL 60439, USA.*

[2]*Nanoscale and Quantum Phenomena Institute, Physics & Astronomy Department, Ohio University, Athens, OH 45701, USA.*

[3]*Center for Nanoscale Materials, Argonne National Laboratory, 9700 S. Cass Ave., Argonne, IL 60439, USA.*

[4]*Department of Physics, Harvard University, Cambridge, MA 02138, USA.*

[5]*Materials Science Division, Argonne National Laboratory, 9700 S. Cass Ave., Argonne, IL 60439, USA.*

*Corresponding Authors: Email: hla@ohio.edu

Magnetism at buried interfaces plays a crucial role in many emerging phenomena, but detection of interfacial magnetism in close proximity to a surface with elemental and chemical sensitivity is a challenging task. Here, we use a low temperature synchrotron x-ray scanning tunneling microscopy to investigate x-ray magnetic circular dichroism and near edge x-ray absorption fine structure of $La_{0.67}Sr_{0.33}MnO_3$ - $LaNiO_3$ superlattices in the absence of a magnetic field. In stark contrast to the weak magnetic signal of Mn when the $La_{0.67}Sr_{0.33}MnO_3$ layers are located on top, a robust x-ray magnetic circular dichroism signal is detected when they are buried underneath the $LaNiO_3$ layers. The near edge x-ray absorption fine structure reveals the valence states of the manganese while the oxygen K-edge x-ray absorption spectra show an increase in hole formation indicating a cogent charge transfer at the $LaNiO_3$/$La_{0.67}Sr_{0.33}MnO_3$ interface. This work demonstrates that scanning tunneling microscopy can be extended to the synchrotron X-ray study of buried interfaces by controlling the sample-tip (e.g., detector) separation in the nanometer regime. The close sample-tip proximity further provides a path toward probing of small lateral areas with zero-field measurements in multi-domain samples.

Interfaces formed by two different materials can exhibit vastly different properties producing many intriguing phenomena, from metal-insulator transition, and superconductivity to interfacial magnetism and Majorana fermions [1-4]. Among them, magnetic interfaces can produce exotic phenomena such as spin-transfer torque[5], and magnetic Skyrmion phases[6], which are promising for applications including data storage, magnetic read heads, and spintronics[7,8]. Understanding magnetic properties of interfaces is vital, and therefore it is desirable to directly probe local interfacial magnetism. Here, we present an experimental scheme to detect local magnetism and chemical components at an interface by combining circularly polarized synchrotron x-rays, and near-edge x-ray absorption fine structure spectroscopy with a scanning tunneling microscope tip acting as a detector, a technique dubbed as synchrotron x-ray scanning tunneling microscopy (SX-STM) [9-11]. SX-STM combines two powerful techniques for materials characterization, synchrotron X-ray and scanning tunneling microscopy, and it has a great potential to detect elemental, chemical, and magnetic signals simultaneously at the atomic scale. Therefore it is desirable to demonstrate the capabilities of SX-STM in detecting interfacial magnetism.

In SX-STM, the STM tip is used as a detector to collect x-ray excited electrons[12,13]. If a polarized x-ray beam is used on magnetic samples, then a spin contrast can be achieved via preferential excitations of majority and minority spins[9]. Here, the spin dependent x-ray excited electrons as well as the cascade of secondary electrons are collected by the STM tip[14]. The process is somewhat similar to the conventional total electron yield (TEY) measurements however the usage of the SX-STM tip located in a close proximity to the surface in SX-STM reduces the lateral sample area for the data collection. SX-STM is a surface sensitive technique and the x-ray excited current is composed of two components; x-ray excited electron tunneling from the states between the Fermi level and the work function, and x-ray ejected electrons with energies above the work functions[14]. Typically, the x-ray excited tunneling current is dominant[14]. Thus in order to access the x-ray excited electrons from the buried interface it is necessary

to eliminate the x-ray excited tunneling from the top surface layer. To circumvent this, the SX-STM tip is positioned ~150 nm above the surface in our experiment, i.e. at the far field. At this tip-sample distance, x-ray excited tunneling does not occur, so that the signal is exclusively composed of x-ray ejected electrons.

The experiments were conducted by using a recently developed low temperature SX-STM system at 110 K substrate temperature in an ultrahigh vacuum environment. The SX-STM system was directly attached to the beamline 4-ID-C of the Advanced Photon Source in Argonne National Laboratory, and left or right circularly polarized (LCP or RCP) monochromatic x-ray beams were incident on tip-sample junction at an angle of ~7±2 degrees with respect to the sample surface (Fig. 1a). Depending on the LCP or RCP, excitations of majority or minority spin components in the sample should be dominant leading to a magnetic contrast for the buried interface (Fig. 1b). The photon flux and energy resolution for the experiment were selected by adjusting the sizes of the entrance and exit slits of the spherical grating monochromator, and energy resolution of 0.1 eV was set by the incident photon energy. The probing depth was determined as ~10 nm based on the escape depth of photoelectrons from the sample. In order to compare XMCD signals for different samples, the SX-STM tip height was adjusted before each experiment by bringing the tip into tunneling regime and then retracting the tip-piezo tube by applying the same voltage. The photo electron current in this experiment was determined by the solid angle seen by the tip, which is a function of the tip-sample distance and the tip coating. We estimate the majority of the recorded photo electrons as originated from the sub-micron surface area underneath the tip based on the solid angle. The x-ray induced photocurrent was recorded by a topographic filter[15] in an ultra-high vacuum environment.

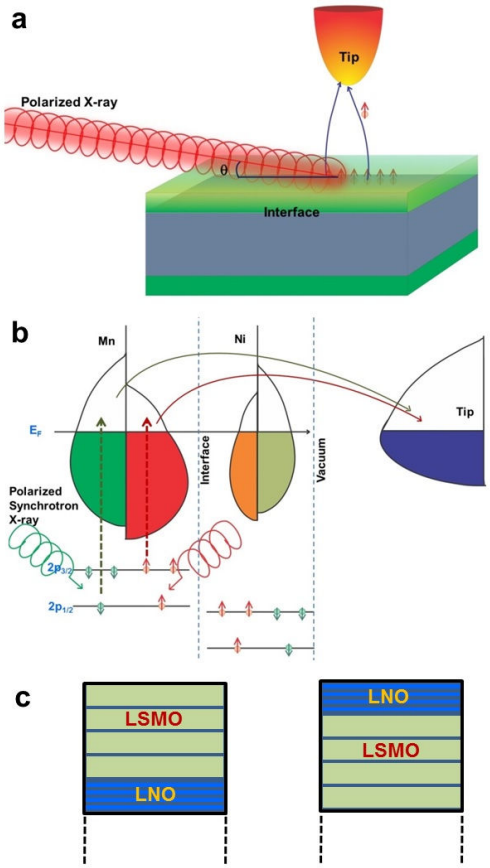

Figure 1. (**a**) A drawing presenting SX-STM-XMCD experimental set-up. A circularly polarized X-ray beam is incident to the sample at θ = 7±2° in our measurements. The photo-current intensity increases when the X-ray induced ejected electrons enter to the tip located above the sample. (**b**) A schematic drawing illustrating spin-sensitive photo ejection of electrons when a circular polarized X-ray is incident at the buried interface. (**c**) LSMO is the top layer in one sample (left) while LNO is the top layer in the other sample (right).

The samples are formed by superlattices of transition metal oxides $La_{0.67}Sr_{0.33}MnO_3$ (LSMO) and $LaNiO_3$ (LNO). Bulk LSMO is a ferromagnetic half-metal at low temperatures[16] while the LNO is a paramagnetic metal[17] and both have perovskite (ABO_3) structures. Magnetic interfaces involving LSMO are well studied due to their potential applications in spintronics, multiferroic field effect, and giant tunnel magnetoresistance read-out devices[18-21]. The LSMO/LNO interface is proposed to exhibit an exchange bias effect[22] induced by an interfacial magnetism. Superlattices comprised of LSMO and LNO were grown on $SrTiO_3$ (STO) substrates along the (001) orientation in the sequence STO/[$(LSMO)_4$/$(LNO)_4$] x 10, and also in the reverse sequence STO/[$(LNO)_4$/$(LSMO)_4$] x 10 for the comparative studies. Thus one

sample has the LNO as the top layer (LNO/LSMO interface) while the other has an LSMO as the top layer (LSMO/LNO interface) (Fig. 1c). Both samples were grown by using ozone assisted molecular beam epitaxy at the Center for Nanoscale Materials at Argonne National Laboratory[23] (supplementary information).

In LSMO and LNO, Ni and Mn are are known to be responsible for the interfacial magnetism[7,16,17]. In bulk LSMO, Mn exhibits magnetism while for the LNO does not show the magnetic behaviors. However, Ni can exhibit magnetism in thin LNO films formed on LSMO[22]. For the experiment, we first measure the sample with LSMO as the top layer, i.e. $(LSMO)_4/(LNO)_4$. To record the Ni STM-XAS signals, the x-ray beam energy is tuned to the Ni L_2 and L_3 region and the spectra are measured with both left and right polarized x-rays. The STM-XAS spectra of Ni reveal a peak at 851.7 eV corresponding to L_3 and two split peaks at 870.2 eV and 869.5 eV for L_2 (Fig. 2a). The split peaks at L_2 are associated with Ni^{2+} and Ni^{3+} oxidation states[22]. Both LCP and RCP signals of Ni L_2 and L_3 appear with similar intensities and the corresponding x-rays magnetic circular dichroism (XMCD) signal obtained by the difference between LCP and RCP shows no apparent features. Therefore no significant magnetization is detected in the burried LNO layers here (Fig. 2a, and 2b). In a previous conventional XMCD study, magnetization of Ni is reported for the LNO grown on LSMO[22]. In order to detect the observed Ni magnetization, an in-plane magnetic field is generally applied to the sample in conventional XMCD measurements[22,23]. In our case, the measurement is performed without an applied magnetic field, and therefore a uniform magnetization sufficient to produce the magnetic signal is not recorded. When the x-ray beam energy is tuned to the Mn L_2 and L_3 region of the top LSMO layer, the Mn L_2 and L_3 peaks are detected at 652.5 eV and 642.1 eV, respectively (Fig. 2c). The Mn L_2 and L_3 peaks are produced by the dipole transition from $2p_{3/2,1/2}$ to unoccupied 3d states and thus, they are sensitive to magnetic characteristics. The STM-XAS

spectra reveal a contrast reversal between the L_2 and L_3 peaks (Fig. 2c) indicating a magnetization. Accordingly, the STM-XMCD data of Mn exhibits the magnetization of LSMO (Fig. 2d).

Next, the STM-XAS experiments are repeated on the $(LNO)_4/(LSMO)_4$ sample. Unlike the LSMO top layer sample, i.e. LSMO/LNO interface, the LNO top layer sample (LNO/LSMO) now reveals a clear intensity reversal between the L_2 and L_3 peaks for LCP and RCP (Fig. 2a). Accordingly, the corresponding STM-XMCD curve exhibits a strong magnetic signal (Fig. 2b). Since LNO does not show magnetic behavior in the bulk, the observed magnetization can be attributed as induced by the LNO-LSMO interface. When the x-ray beam energy is tuned to the Mn L-edge energy range, the Mn L_2 and L_3 signals from the buried LSMO layer are detected. The recorded signals again reveal a clear intensity reversal of L_2 and L_3 peaks between LCP and RCP (Fig. 2c). The corresponding STM-XMCD data further confirms a magnetization in the buried LSMO layer (Fig. 2d). Comparison between the Mn STM-XMCD data of the two interfaces (Fig. 2d) clearly shows a stronger magnetic signal in the (LNO)/(LSMO). Since we are detecting the photocurrent with the STM tip, one would expect a stronger Mn STM-XMCD signal in (LSMO)/(LNO) because the LSMO layer here is located closest to the tip. The surprising observation of a stronger Mn STM-XMCD signal from the buried LSMO layer located ~1.5 nm under the top surface LNO layer indicates a robust magnetization at the LNO/LSMO interface. This is also in agreement with a strong Ni STM-XMCD signal in (LNO)/(LSMO).

To understand the observed interfacial magnetism, we determine the near edge X-ray absorption fine structures (NEXAFS) of Mn L_3 edge of the (LSMO)/(LNO) and (LNO)/(LSMO) (Fig. 3a) using SX-STM tip, which are recorded by ramping the X-ray beam energy with 0.1eV intervals. A number of features are observed in the STM-NEXAFS spectra (Fig. 3a), which are labeled as; **a** (640.1 eV), **a'** (640.5 eV), **b** (641.3 eV), **b'** (641.9 eV), **c** (642.4 eV), and **c'** (643.5 eV). The excitation of the 2p to 3d states in transition

metals such as Mn obeys dipole selection rules and are influenced by multiplet effects[24]. The observed energies are well in agreement with the conventional NEXAFS spectra of Mn valence states in different compounds[25-28], and thus we can assign **a**, and **a'** to the divalent Mn^{2+}, while the **b**, **b'**, **c** and **c'** are attributed to the Mn^{3+}/Mn^{4+} components. In addition, we have observed two more peaks; 1 (639.3 eV), and 1' (639.7 eV) (Fig. 3a). The energies of these peaks are slightly lower than the known energies of Mn^{2+} and they could be either pre-edge states or previously unassigned Mn^{2+} multiplets. Conparing the STM-NEXAFS spectra in Fig. 3a, it is clearly evident that the LSMO/LNO interface exhibits a higher intensity for the Mn^{2+} components (lower energy peaks) while the LNO/LSMO interface shows a high intensity for the Mn^{3+}/Mn^{4+} components (higher energy peaks). This is also in agreement with the STM-XMCD data where the spin down Mn STM-XMCD signal is centered at 640.7 eV in LSMO/LNO while it is located at 642.3 eV in LNO/LSMO interface (Fig. 2d).

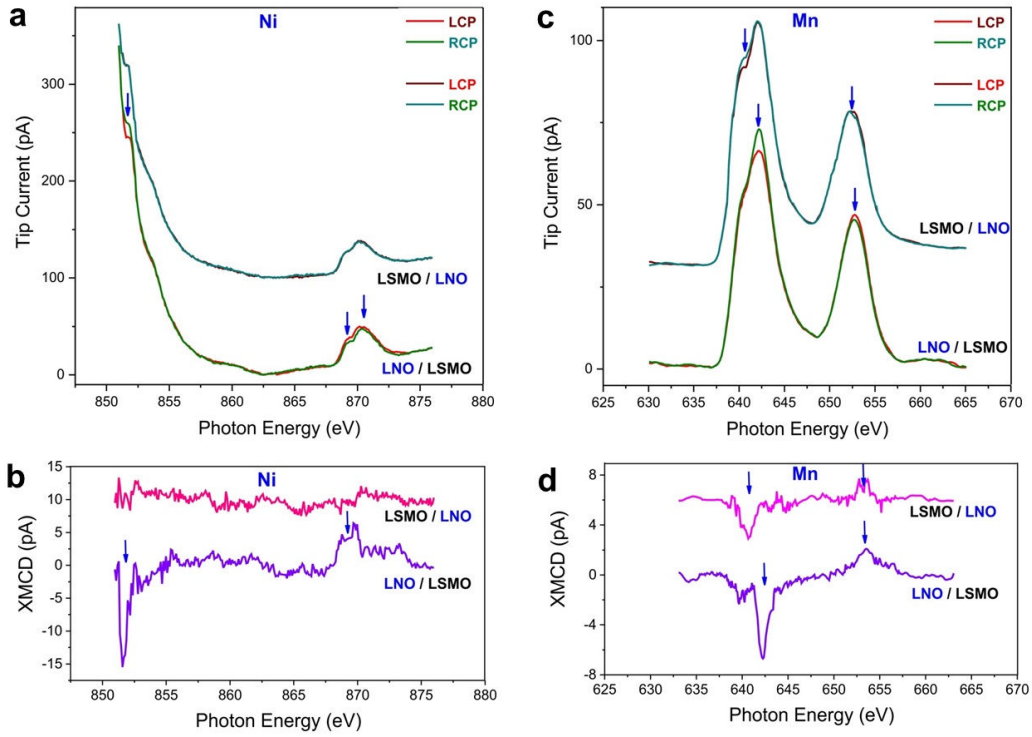

Figure 2. (**a**) STM-XAS spectra of Ni acquired for LSMO/LNO (top) and LNO/LSMO (bottom) interfaces. (**b**) STM-XMCD spectra of Ni exhibits magnetism in the LNO/LSMO interface while no magnetic signal is observed for LSMO/LNO interface. (**c**) STM-XAS spectra of Mn acquired for LSMO/LNO (top) and LNO/LSMO (bottom) interfaces. (**d**) The STM-XMCD spectra of Mn show a larger magnetization for the LNO/LSMO then LSMO/LNO interface. (Blue arrows indicate magnetic signals).

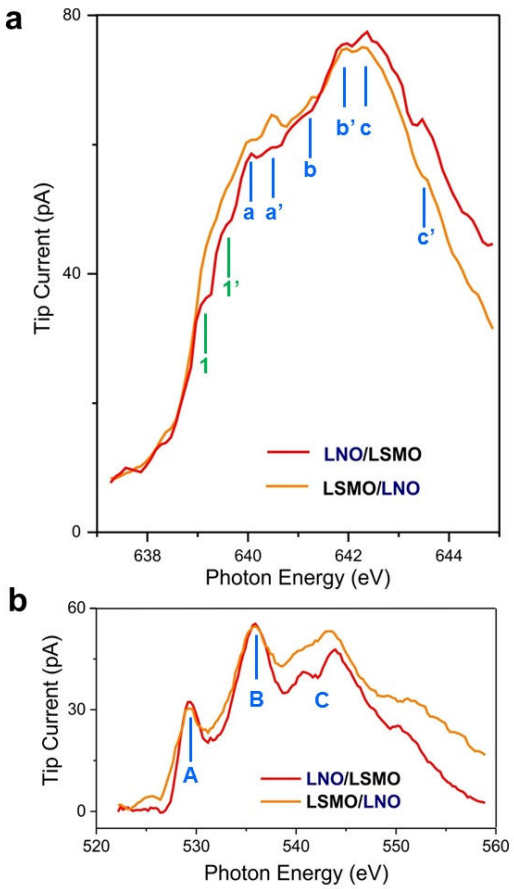

Figure 3. (**a**) NEXAFS spectra of Mn L_3 edge corresponding to LNO/LSMO (red) and LSMO/LNO (orange) interfaces. The orange spectrum is dominant at the lower energies while the red spectrum becomes dominant at the higher intensities. (**b**) Oxygen K edge spectra of LNO/LSMO (red) and LSMO/LNO (orange) interfaces. Here, the red spectrum has a higher intensity then the orange spectrum at 'A', which belongs to O 2p-metal 3d hybridized states.

To further confirm the observed Mn valence state concentrations, we analyze the oxygen (O) K-edge spectra of the two interfaces. Excitation of O 1s states to 2p can provide alternative information because the O 2p states are strongly hybridized with the metal 3d states[25,29,30]. The STM-XAS spectra of the O K-edge (Fig. 3b) show sharp peaks at 529.4 eV (A) and 535.9 eV (B). The region labeled as 'C' has a broader peak at 543.4 eV for LSMO/LNO while two peaks at 540.7 eV and 543.9 eV for LNO/LSMO interface, respectively. The peak at 'B' corresponds to the hybridization with La/Sr while the peak or peaks at the region 'C' are related to the states with the sp hybridizations[25]. The most important information can be obtained from the peak at 'A', which corresponds to the hybridization of O 2p with metal '*d*' states.

Here, the LNO/LSMO has a higher intensity peak than that shown by the LSMO/LNO (Fig. 3b) interface. This means that the LNO/LSMO interface produces more holes, which allows to accept more excited electrons from the O 1s states thereby enhancing the photocurrent intensity. This is very well in agreement with the higher intensity peaks of Mn^{3+}/Mn^{4+} components found in LNO/LSMO as compared to LSMO/LNO interface.

Unlike conventional XMCD experiments, we have not applied any magnetic field to the sample in our experiments. Magnetization at the interface generally forms domains, and the magnetic signal is averaged out for the large sample area used to measure by the conventional XMCD. Thus an applied magnetic field is generally required to reorient the sample magnetization. However, the SX-STM detects the signal from a smaller region then the conventional XMCD set-up and therefore the magnetic signal can be measured without an external applied magnetic field. In the absence of a magnetic field, the observed magnetizations of Ni L_2 and L_3 in the top LNO layers in $(LNO)_4/(LSMO)_4$ sample can be attributed as solely due to the interfacial magnetism, which is induced by the charge transfer at the LNO/LSMO interface. There is a controversy in the literature concerning the origin of LNO/LSMO interfacial magnetism as induced by either a spin glass state[31] or interfacial charge transfer[22,32]. It is known that the Ni^{3+} and Mn^{3+} ions are dominant in the bulk LNO[33] and LSMO[34], respectively. At the interface, the charge transfer from Mn to Ni occurs by donating an electron that results in the transformation of Ni^{3+} to Ni^{2+} while Mn^{3+} becomes Mn^{4+} [22,33]. Our results suggest a stronger magnetization of the LNO/LSMO interface than the LSMO/LNO interface. It has been proposed that the interfacial strain induced by the top LNO layer cap onto the LSMO layers underneath can influence the resultant interfacial magnetic behavior[32]. Such interfacial strain would alter the orbital asymmetry and the Fermi level alignment at the interface. Our finding shows that not only LSMO layers in $(LNO)_4/(LSMO)_4$ sample have stronger magnetization but also the LNO layers become magnetic. This

suggests that the interfacial strain induced by the top LNO layer onto the LSMO layer underneath can have a profound influence in stabilizing magnetism in both materials. Our results further suggest that LNO is a good cap layer for LSMO to maintain its magnetic behavior at least in the thin-film regime, and thus impacting its potential applications.

In summary, the measurements of a buried magnetism by means of local XMCD signals in the absence of a magnetic field, and the detection of the chemical components at the interface by means of NEXAFS using an STM tip have been demonstrated. This work proves the feasibility of these techniques with SX-STM and provide an important groundwork for future research directions where synchrotron x-ray characterizations of materials will be able to perform using a scanning tunneling microscope set-up potentially down to ultimate atomic scale.

SUPPLEMENTARY MATERIALS

X-ray reflectivity (XRR) and Parratt fit for an $[(LSMO)_4/(LNO)_4]$ x 10 superlattice grown on $SrTiO_3$.

ACKNOWLEDGMENT

Use of the Advanced Photon Source and the Center for Nanoscale Materials was supported by the U.S. Department of Energy, Office of Science, Office of Basic Energy Sciences, under contract DE-AC02-06CH11357. V.R. acknowledges the Office of Science Early Career Research Program through the Division of Scientific User Facilities, Office of Basic Energy Sciences of the U.S. Department of Energy through Grant SC70705. H.C. and S.W.H acknowledges the support of U.S. Department of Energy, Office of Science, Office of Basic Energy Sciences, under contract DE-FG02-02ER46012 for the SX-STM spectroscopic data analysis. J.H. and A.B acknowledge support from the U.S. Department of Energy, Office of Basic Energy Science, Materials Science and Engineering Division.

REFERENCES

1. H. Y. Hwang, Y. Iwasa, M. Kawasaki, B. Keimer, N. Nagaosa, Y. Tokura. *Emergent phenomena at oxide interfaces*. Nat. Mater. **11**, 103-113 (2012).

2. H. Alves, A.S. Molinari, H.X. Xie, A.F. Morpurgo. *Metallic conduction at organic charge transfer interfaces.* Nat. Mater. **7**, 574-580 (2008).

3. J. Chakhalian, J. W. Freeland, A.J. Millis, C. Panagopoulos, J. M. Rondinelli. *Colloquium: Emergent properties in plane view: Strong correlations at oxide interfaces*. Rev. Mod. Phys. **86,** 1189 (2014).

4. A. R. Akhmerov, J. Nilsson, C. W. J. Beenakker. *Electrically detected interferometry of Majorana Fermions in a topological insulator.* Phys. Rev. Lett. **102**, 216404 (2009).

5. I.M. Miron, G. Gaudin, S. Auffret, B. Rodmacq, A. Schuhl, S. Pizzini, J. Vogel, P. Gambardella. *Current-driven spin torque induced by the Rashba effect in a ferromagnetic metal layer.* Nat. Mater. **9**, 230-234 (2010).

6. B. Dupe, M. Hoffmann, C. Paillard, S. Heinze. *Tailoring magnetic skyrmions in ultra-thin transition metal films.*Nat. Comm. **5**, 4030 (2014).

7. M. Gibert, P. Zubko, R. Scherwitzl, J. Íñiguez, J.-M. Triscone. *Exchange bias in $LaNiO_3$–$LaMnO_3$ superlattices.* Nat. Mater. **11**, 195-198 (2012).

8. C. Pollak, K. Reichmann, H. Hutter. *Comparative study of LNO, LSCO and LSMO as electrode layers for microelectronic capacitors by dynamic SIMS.* Surf. Coat. Technol. **150**, 119-124 (2002).

9. M. Cummings, N. Shirato, H. Kersell, H. Chang, D. Rosenmann, J. W. Freeland, D. Miller, S.-W. Hla, and V. Rose. *Controlled modulation of hard and soft X-ray induced tunneling currents utilizing coaxial metal-insulator-metal probe tips*. J. Appl. Phys. **121**, 015305 (2017).

10. V. Rose, K. Wang, T. Chien, J. Hiller, D. Rosenmann, J.W. Freeland, C. Preissner, S.-W. Hla. *Synchrotron X-ray Scanning Tunneling Microscopy: Fingerprinting Near to Far Field Transitions on Cu(111) Induced by Synchrotron Radiation*. Adv. Funct. Mater. **23**, 2646-2652 (2013).

11. N. Shirato, M. Cummings, H. Kersell, Y. Li, B. Stripe, D. Rosenmann, S.-W. Hla, V. Rose. *Elemental Fingeroprinting of Materials with Sensitivity at the Atomic Limit*. Nano Lett. **14**, 6499-6504 (2014).

12. A. Saito, J. Maruyama, K. Manabe, K. Kitamoto, K. Takahashi, K. Takami, M. Yabashi, Y. Tanaka, D. Miwa, M. Ishii, Y. Takagi, M. Akai-Kasaya, S. Shin, T. Ishikawa, Y. Kuwahara, M. Aono. *Development of a Scanning Tunneling Microscope for in Situ Experiments with a Synchrotron Radiation Hard-X-ray Microbeam*. J. Synchrotron Rad. **13**, 216-220 (2006).

13. T. Okuda, T. Eguchi, K. Akiyama, A. Harasawa, T. Kinoshita, Y. Hasegawa, M. Kawamori, Y. Haruyama, S. Matsui. *Nanoscale Chemical Imaging by Scanning Tunneling Microscopy Assisted by Synchrotron Radiation*. Phys. Rev. Lett. **102**, 105503 (2009).

14. H. Kersell, N. Shirato, M. Cummings, H. Chang, D. Miller, D. Rosenmann, S.-W. Hla, V. Rose. *Detecting element specific electrons from a single cobalt nanocluster with synchrotron X-ray scanning tunneling microscopy*. Appl. Phys. Lett. in press (2017).

15. K. Wang, D. Rosenmann, M. Holt, R. Winarski, S.-W. Hla, V. Rose. *An Easy-to-Implement Filter for Separating Photo-Excited Signals from Topography in Scanning Tunneling Microscopy*. Rev. Sci. Instrum. **84**, 063704 (2013).

16. C. Ma, Z. Yaqng, S. Picozzi. *Ab initio electronic and magnetic structure in $La_{0.66}Sr_{0.33}MnO_3$: Strain and correlation effects*. J. Phys.: Condens. Matter **18**, 7717-7728 (2006).

17. L. Guan, B. Liu, L. Jin, J. Guo, Q. Zhao, Y. Wang, G. Fu. *Electronic structure and optical properties of LaNiO3: First-principles calculations*. Solid. Stat. Comm. **150**, 2011-2014 (2017).

18. V. Garcia, S. Fusil, K. Bouzehouane, S. Enouz-Vedrenne, N. D. Mathur, A. Barthe´le´my, M. Bibes. *Giant tunnel electroresistance for non-destructive readout of ferroelectric states*. Nature **460**, 81-84 (2009).

19. V. Garcia, M. Bibes, L. Bocher, S. Valencia, F. Kronast, A. Crassous, X. Moya, S. Enouz-Vedrenne, A. Gloter, D. Imhoff, C. Deranlot, N. D. Mathur, S. Fusil, K. Bouzehouane, A. Barthélémy. *Ferroelectric control of spin polarization*. Science **327**, 1106-1110 (2010).

20. S. M. Wu, S. A. Cybart, P. Yu, M.D. Rossell, J.X. Zhang, R. Ramesh, R. C. Dynes. *Reversible electric control of exchange bias in a multiferroic field-effect device*. Nature Mater. **9**, 756-761 (2010).

21. C. Barraud, P. Seneor, R. Mattana, S. Fusil, K. Bouzehouane, C. Deranlot, P. Graziosi, L. Hueso, I. Bergenti, V. Dediu, F. Petroff, A. Fert. *Unravelling the role of the interface for spin injection into organic semiconductors*. Nature Phys. **6**, 615-620 (2010).

22. J.C. Rojas Sanchez, B. Nelson-Cheeseman, M. Granada, E. Arenholz, L.B. Steren. *Exchange-bias effect at $La_{0.75}$ $Sr_{0.25}$ MnO_3/$LaNiO_3$ interfaces*. Phys. Rev. B **85**, 094427 (2012).

23. J.D. Hoffmann, B.J. Kirby, J. Kwon, G. Fabbris, D. Meyers, J.W. Freeland, I. Martin, O.G. Heinonen, P. Steadman, H. Zhou, C.M. Schleputz, M.P.M. Dean, S.G.E. te Velthuis, J.-M. Zho, A. Bhattacharya. *Oscillatory nonlinear magnetism induced by interfacial charge transfer in superlattices composed of metallic oxides*. Phys. Rev. X. **6**, 041308 (2016).

24. M. Abbate, F.M.F. de Groot, J.C. Fuggle, A. Fujimori, O. Strebel, F. Lopez, M. Domke, G. Kaindl, G.A. Sawatzky, M. Takano, Y. Takeda, H. Eisaki, S. Uchida. *Controlled-valence properties of La_{1-x} Sr_x FeO_3 and La_{1-x} Sr_x MnO_3 studied by soft-x-ray absorption spectroscopy.* Phys. Rev. B **46**, 4511-4519 (1992).

25. H.W. Nesbitt, D. Banerjee. *Interpretation of XPS Mn (2p) spectra of Mn oxyhydroxides and constraints on the mechanism of MnO2 precipitation*. Am. Mineralogist **83**, 305-315 (1998).

26. G. Anjum, R. Kumar, S. Mollah, P. Thakur, S. Gautam, K. H. Chae. *NEXAFS studies of $La_{0.8}$ $Bi_{0.2}$ Fe_{1-x} Mn_x O_3($0.0 \leq x \leq 0.4$) multiferroic system using x-ray absorption spectroscopy*. J. Phys. D: Appl. Phys. **44** 075403 (2011).

27. P. Thakur, K. H. Chae, J.-Y. Kim, M. Subramanian, R. Jayavel, K. Asokan. *X-ray absorption and magnetic circular dichroism characterizations of Mn doped ZnO.* Appl. Phys. Lett. **91**, 162503 (2007).

28. M. Khan, E. Suljoti, A. Singh, S.A. Bonke, T. Brandenburg, K. Atak, R. Golnak, L. Spiccia, E.F. Aziz. *Electronic structural insights into efficient MnO_x catalysts*. J. Mater. Chem. A. **2**, 18199-18203 (2014).

29. M. Abbate, G. Zampieri, F. Prado, A. Caneiro, J.M. Gonzalez-Calbet, M. Vallet-Regi. Electronic structure and metal-insulator transition in LaNiO3-δ. Phys. Rev. B **65**, 115101 (2002).

30. F.M.F. de Groot, M. Grioni, J.C. Fuggle, J. Ghijsen, G.A. Sawatzky, H. Petersen. *Oxygen 1s x-ray-absorption edges of transition-metal oxides.* Phys. Rev. B **40**, 5715-5723 (1989).

31. G.-W. Zhou, X.-F. Guan, Y.-H. Bai, Z.-H. Quan, F.-X. Jiang, X.-H. Xu. *Interfacial spin glass state and exchange bias in the epitaxial $La_{0.7}Sr_{0.3}MnO_3$/$LaNiO_3$ bilayer*. Nano. Res. Lett. **12**, 330 (2017).

32. J. Peng, C. Song, F. Li, B. Cui, H. Mao, Y. Wang, G. Wang, F. Pan. *Charge transfer and orbital reconstruction in strain-engineered (La, Sr)MnO_3/$LaNiO_3$ heterostructures.* ACS Appl. Mater. Interfaces **7**, 17700-17706 (2015.)

33. K. Sreedhar, J.M. Honig, M. Darwin, M. McElfresh, P.M. Shand, J. Xu, B.C. Crooker, J. Spalek. *Electronic properties of the metallic perovskite LaNiO3: Correlated behavior of 3d electrons.* Phys. Rev. B **46**, 6382-6386 (1992).

34. J.L. Garcia-Munoz, M. Suaaidi, J. Fontcuberta, J. Rodriguez-Carvajal. *Reduction of the Jahn-Teller distortion at the insulator-to-metal transition in mixed valence manganites.* Phys. Rev. B **55**, 34-37 (1997).